Heat and Mass Transfer Research Journal
Vol. 2, No. 2; 2018
Published by CanSRG
http://cansrg.com/journals/hmtrj/

An Empirical Correlation for the Void Fraction at Critical Heat Flux Close to the Wall for Subcooled Flow Boiling of a Low Boiling Refrigerant

Moritz Bruder* and Thomas Sattelmayer
Lehrstuhl fur Thermodynamik, Technische Universitat Munchen, Garching, Germany

Abstract

The occurrence of critical heat flux is still one of the most relevant phenomena in the research of boiling heat transfer. Despite a multitude of available models, the true mechanism leading to the departure from nucleate to film boiling remains to be fully understood. Because of its high technical relevance, there exist many tools to predict critical heat flux. Although these tools may provide sufficient accuracy for a limited number of technical applications, their universal applicability is still limited. In the case of one of the most current boiling models in computational fluid dynamics, this could be partly attributed to an unphysical switch mechanism marking the departure from nucleate boiling based on a constant value of the local void fraction at the wall. In this study, void fraction in the immediate vicinity of a copper heater was measured in a flow boiling test rig using a refrigerant with a low boiling point for a wide range of operating parameters. It was observed that void fraction is largely influenced by inlet subcooling, even at very small distances away from the heated surface and that it is far from constant. Based on these measurements, a new correlation for the void fraction close to the wall at critical heat flux was developed to improve the current predictive capabilities until a unifying model for the prediction of critical heat flux is developed. The new correlation shows good agreement with the measured void fractions close to the wall at critical heat flux.

Nomenclature

A	Boiling area partition
G	Mass flux density
h	Heat transfer coefficient
$\dot{m}$	Mass flux
n	Number of recorded samples per time interval
Q	Heat flux
$\dot{q}$	Heat flux density
R^2	Coefficient of determination
sr	Sample rate
t	Time of averaging interval
U	Voltage

Greek symbols

α	Void fraction
Δh	Specific enthalpy difference
ΔT	Temperature difference
ΔH_f	latent heat of solidification

Superscripts

calc	Calculated value
conv	Convection
crit	Critical heat flux
evap	Evaporation
exp	Experimentally
g	Gaseous phase
l	Liquid phase
quench	Quenching
sub	Subcooling

Submitted: June 15, 2018 Accepted: August 17, 2018

sup	Superheat	W	Wall/boiling surface
th	Threshold		

1. Introduction

Departure from nucleate boiling (DNB) and the occurrence of critical heat flux (CHF) are still one of the most investigated phenomena in boiling heat transfer. Many conceptualizations, correlations and empirical or mechanistic models have been proposed over the last decades. The need to model CHF is of high technical relevance to for example nuclear reactor safety or the cooling of high-power electronics. Several tools have been developed to address this challenge. The underlying models of these tools are either based on mechanistic ideas or empirical models and correlations.

1.1. Modeling of CHF

Although mechanistic macrolayer models such as the Bubble Crowding Model [1, 2], the Sublayer Dryout Model [3, 4] and the Interfacial Lift Off Model [5] were developed based on physical mechanisms, their universal prediction accuracy is still low. Based on a detailed analysis in [6] and [7], the aforementioned models were implemented numerically in MATLAB® by the authors to assess their performance when being subjected to different experimental configurations. The analysis showed that a change in fluid properties had in many cases a catastrophic effect on the accuracy of the models. Based on the work by Theofanus et al. [8, 9] research in the past decades has shifted away from the macrolayer approaches of the classical mechanistic models. Instead, focus has been laid on microlayer and dry spot rewetting phenomena on the boiling surface. While exemplary progress has been made in uncovering the processes leading to DNB, for example in [10–15], these findings alongside the classical mechanistic models have so far been used mainly in academia. Under the precondition of a correct physical representation of the trigger mechanism at CHF, mechanistic models could offer a higher validity than purely empirical correlations or empirical models. However, industry mostly relies on the latter in combination with computational fluid dynamics (CFD) [16–18]. CFD inherently circumvents the disadvantage of the often applied integral modeling of a highly local phenomenon by classical mechanistic models. One of the most recent tools used in this context is the extended wall boiling model (eRPI) as introduced by Lifante et al. [18] based on the model by Kurul and Podowski [19] from Rensselaer Polytechnical Institute. This empirical model partitions the heat flux transferred over the boiling surface according to Eq. (1). Several advancements or new ideas [21] have been proposed since the model's initial proposal. However, in an industrial context, the eRPI model is still the state of the art tool for CHF analysis.

$$\dot{Q}_W = \dot{Q}_{conv,g} + \dot{Q}_{conv,1} + \dot{Q}_{quench} + \dot{Q}_{evap} = f(\alpha) A_g h_{conv,g}\left(T_W - T_g\right)$$
$$+[1 - f(\alpha)] A_1 h_{conv,1}(T_W - T_1) + [1 - f(\alpha)] A_g \Delta h_{quench}(T_W - T_1) + \dot{m}_{evap} \Delta h_{evap} \quad (1)$$

Borrowing from the Bubble Crowding Model, the local void fraction at the wall has found its way into the eRPI model, functioning as the CHF indicator when a certain user-defined threshold is reached. This is realized by using the blending function f (α) in Eq. (2) with a fixed critical void fraction value of αcrit. Depending on the local void fraction at the wall and the value of the critical void fraction, this function steadily blends over between the respective heat flux partitions. This introduces a limiting mechanism enabling the eRPI to model the occurrence of CHF.

$$f(\alpha) = \begin{cases} 0.5\left(\frac{\alpha}{\alpha_{crit}}\right)^{20\alpha_{crit}} & \text{for } \alpha < \alpha_{crit} \\ 1 - 0.5\, exp[-20(\alpha - \alpha_{crit})] & \text{for } \alpha \geq \alpha_{crit} \end{cases} \quad (2)$$

As shown in Fig. 1(a), the slope of $f(\alpha)$ is rather steep around the critical void fraction. Thus, this parameter heavily influences the calculation of wall heat flux. Even though this mechanism may be viable for the combination of fluids, geometries and operating parameter ranges from which this critical value was derived, it was observed that the void fraction at CHF is far from constant. Fig. 1(b) shows void fraction measurements plotted over the wall superheat with respect to inlet subcooling with the experimental setup described in the following section. These measurements were conducted 1 mm away from the boiling surface, where void fraction at CHF was observed to vary between 35 % and 75 % depending on bulk flow inlet subcooling. This indicates a coupling between the region in the immediate vicinity of the heater wall and the bulk flow properties. Subsequently, a universal fixed value for the void fraction at CHF as used in the eRPI model appears to be invalid.

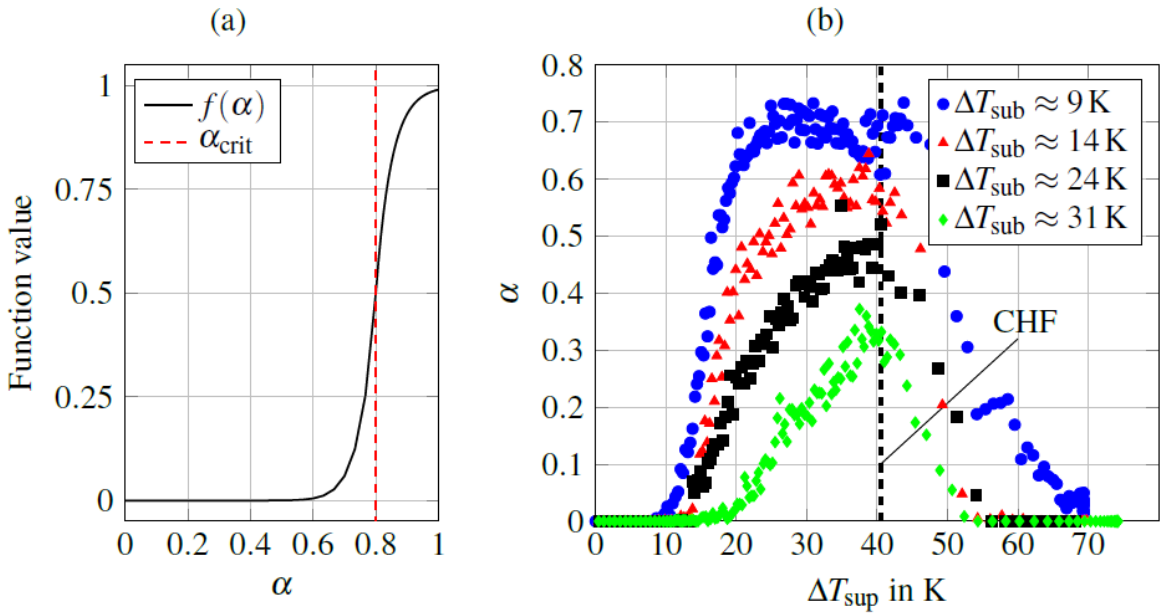

Figure 1. (a) Blending function of the eRPI model with a critical void fraction value of α_{crit}= 0.8, (b) Void fraction measurements along the entire boiling curve for different subcoolings at $G \approx 1000\,kgm^{-2}\,s^{-1}$ at a distance of 1 mm away from the boiling surface.

With a multitude of available mechanisms, models and opinions about the flow topology at CHF, it is evident that the need for a comprehensive and universal model for the transition from nucleate to film boiling persists. Moreover, despite exemplary theoretical and experimental advancements, the physical mechanism of CHF remains to be fully understood. This can only be done by conducting detailed complementary fundamental experiments to gain new insight into the processes leading to DNB and to further identify the triggers of CHF. However, available tools should be improved meanwhile to offer a greater universality than currently available. As CFD in combination with the eRPI model is the current state of the art tool regarding the simulation of boiling phenomena, a more precise switch mechanism appears to have significant potential to

expand the accuracy of CHF simulation until a comprehensive model based on the most recent research is developed. This paper therefore introduces a new correlation for the void fraction at the wall at CHF in subcooled flow boiling for low boiling refrigerants to be used instead of a fixed value for α_{crit} in the eRPI model.

2. Experimental approach

To obtain void fraction data at CHF at the wall, experiments with a coolant were conducted at mass flux densities ranging from 500 kg m^{-2} s^{-1} to 2000 kgm^{-2} s^{-1} and subcoolings ranging from 4 K to 31 K. This section describes the experimental setup and procedure used to obtain wall heat flux, wall temperature and void fraction values at CHF.

2.1. Boiling test rig

The boiling test rig used for the experiments consists of a fluid loop with a vertically oriented test section, as shown schematically in Fig. 2. The fluid is circulated through the loop by a centrifugal pump. A preheater is used to control the subcooling of the fluid. Flow straighteners ensure a homogeneous flow free from any secondary flows at the inlet of the test section, which was confirmed via particle image velocimetry measurements. After passing through the test section, the two-phase flow is condensed and cooled down in a counter flow heat exchanger before it enters a deaerator with a reflux condenser. The reflux condenser is open to the environment, ensuring atmospheric pressure at the highest point of the test rig. Several bypasses allow the filtering of particles and enable the filling and the removal of fluid. Temperature measurements at positions 1 and 2 in Fig. 2 determine the amount of preheater power needed and the subcooling of the fluid. At position 2 and 3 pressure transducers can be fitted to determine the inlet pressure of the test cell and for tightness testing of the test rig to minimize the loss of expensive working fluid.

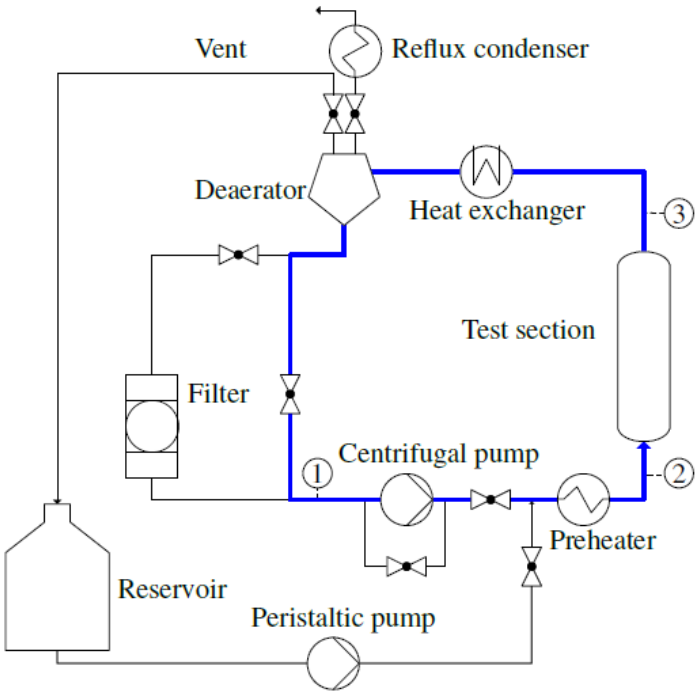

Figure 2. Schematic of the boiling loop (main flow loop is marked in bold blue).

Fig. 3 shows a three-dimensional view of the test section. It has a total length in flow direction of 500 mm and has a square cross section of 40 mm by 40 mm. Heat is transferred into the test section by a copper bar, which is part of a bigger copper block. Heat is provided by twelve heater cartridges with a combined maximum power of 2.4 kW inserted into the copper block. The heater is mounted flush in one of the walls of the test chamber and is placed in the axis of symmetry of the wall. The area of the boiling surface is 15 mm by 200 mm. The upstream end of the heater begins at 150 mm after the inlet of the test section. The inlet pressure of the test section was measured to be 1.15 bar. To reach critical heat flux and capture the transition to fully developed film boiling, a fluid with a low boiling temperature is used in the experiments. The fluid chosen is Novec 649 by 3M, a dodecaflouromethylpentatone with a boiling point of 49 °C and an enthalpy of evaporation of 88 kJ kg^{-1} at ambient pressure. The fluid is similar in its chemical and physical properties to the often-used coolant FC-72. Its main physical properties at ambient conditions in comparison to water are given in Table 1.

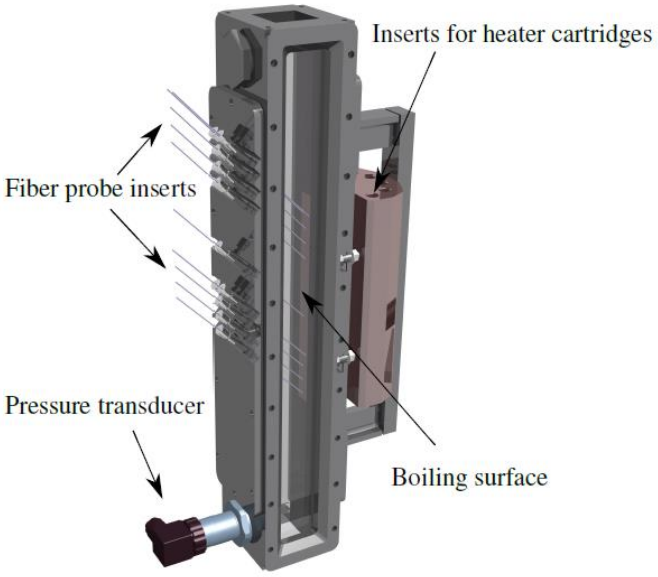

Figure 3. Three-dimensional view of the test section.

Table 1. Main fluid parameters at ambient conditions of Novec 649 in comparison to water.

Quantity	Novec 649	Water	Unit
Boiling point	49	100	°C
Enthalpy of vaporization	88	2337	kJ kg^{-1}
Specific heat	1103	4182	J kg^{-1} K^{-1}
Liquid density	1616	998	kg m^{-3}
Vapor density	12.6	0.59	kg m^{-3}
Surface tension	10.8	72.8	mN m^{-1}
Critical temperature	442	647	K
Critical pressure	1.88	22.12	MPa

2.2. Measurement techniques

To measure heat flux and wall temperature, there are three rows of four thermocouples each, which are mounted inside the heater below the boiling surface. Heat flux is calculated using the law of Fourier and surface temperature is extrapolated linearly using the temperature gradient between the thermocouples in each respective row. A numerical analysis of the heat transfer processes inside the heater showed no substantial heat transfer inside the heater in the direction of flow. Therefore, this approach to obtaining heat flux and wall temperature values was deemed applicable. Fig. 4 shows a detailed view of the thermocouple positions within the heater. Thermocouples of type K are used at distances of 9 mm, 17 mm and 25 mm below the heater surface, while the ones closest to the boiling surface are of type T. The acquisition frequency for all temperature measurements in the system was 2 Hz.

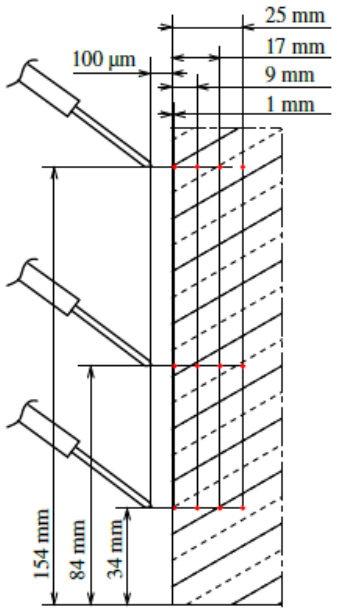

Figure 4. Detailed schematic view of the positions of the fiber probes (not to scale) above the boiling surface and the thermocouples mounted inside the heater.

Three optical fiber probes were used to measure void fraction at the wall. This technique has been used by many researchers in multiphase flow experiments, for example [22–28]. Based on the law of Snellius [29], these probes detect the change in refractive index at the tip of the glass fiber, where light is either reflected within the fiber or projected into flow channel depending on the phase present at the tip. The probe tip consists of a glass fiber with a core diameter of 50 µm and has a conical shape at an angle of approximately 45°. The fiber is embedded in a steel ferrule for increased mechanical stability. The measurement apparatus consists of the probe tip, a fiber coupler, a photodiode and an amplifier as well as an analog to digital converter running at 60 kHz per channel for each individual fiber. A fiber-coupled laser source was used to power the whole system. This ensured a good signal to noise ratio and minimized unwanted interference due to the closed beam path. Void fraction is calculated using a moving average approach with a phase indicator function (PIF) according to Eq. (3) and Eq. (4) respectively. This approach has been used similarly in other works, for example [6, 30, 31]. For the purpose of this study, n = 30000 was used,

which for a sample rate of *sr* = 60 kHz equates to an averaging interval of 0.5 s. This interval length was chosen to match the acquisition frequency of temperature data of 2 Hz.

$$\alpha(t) = \frac{1}{n}\sum_{i=1}^{n} PIF\left[t - \left(\frac{n-i}{sr}\right)\right] \tag{3}$$

$$f(\alpha) = \begin{cases} 1 & \forall\, U > U_{th} \\ 0 & \forall\, U \leq U_{th} \end{cases} \tag{4}$$

The optical fiber probes were inserted into the flow channel from the left-hand side of the test cell as depicted in Fig. 3 at an angle of 42°C. The probes were positioned at 100 µm above the heater surface at the locations of the thermocouple rows in the heater using a traversing mechanism with an accuracy of ±5 µm, which was verified with microscopic images for each measurement. This allowed for the synchronous and locally coupled measurement of heat flux data, temperature data and void fractions. Due to the high thermal conductivity of the copper heater, boiling for each operating condition started at the same position at the upstream end of the heater strip in the channel and no variance regarding the location of the onset of boiling on the heater could be observed. Hence, the fixed optical fiber probe positions captured the boiling process at similar stages along the direction of flow allowing for the comparison of void fraction data for different operating parameters.

2.3. Measurement procedure

Experiments were conducted transiently. It was shown previously in [32] that the system be- haves quasi-statically and results from transient experiments match steady state experiments for this setup. To ensure consistent surface properties, the boiling surface was polished after every fourth experiment using a 2500-grit paper. Following polishing the first run was discarded to eliminate effects of non-condensables. This way, a very good repeatability of the experimental data was achieved. The experimental procedure for each transient experiment was as follows.

1. The heater is at or close to ambient conditions and there is no boiling activity on the heater surface.
2. The preheater is switched on and the system is heated up to the desired subcooling. 3.Upon reaching the desired subcooling, the fiber probes are positioned at 100 µm above the boiling surface at the positions of the thermocouple rows for each experiment.
3. Once the probes are positioned the heater cartridges are switched on. Simultaneously, data acquisition is started and the system goes through one complete boiling cycle from single phase convection to fully developed film boiling. The heater cartridges and data acquisition equipment is switched off when the Leidenfrost point is reached after CHF occurred and heat flux begins to increase again.
4. Afterwards, the system is cooled down until the initial conditions are achieved.

2.4. Uncertainty

In calibration experiments, the deviation between any thermocouples used in the test rig at ambient conditions were measured to be approximately 0.2 K. The positioning accuracy of the thermocouples within the copper bar due to manufacturing inaccuracies as depicted in Fig. 4 was assumed to be better than 0.1 mm. A Gaussian error propagation was calculated based on these

values. For mass flux density, a statistical fluctuation of 20 kg m^{-2} s^{-1} was tolerated as reference experiments had shown that the influence on CHF and wall temperature is small. Videometric calibration experiments were done during the development phase of the fiber probe tips. These experiments showed good agreement between the signal from the fiber probes and the observed trajectories of bubbles touching the probe tips and matched typical errors commonly found in literature (e.g.: [23, 28, 33]). The uncertainties of all presented quantities in this paper are summarized in Table 2.

Table 2. Overview of uncertainties of measured quantities.

Quantity	Uncertainty	Unit
Heat flux	± 10.7	$kW m^{-2}$
Wall temperature	± 0.9	K
Subcooling	± 0.2	K
Mass flux density	± 20	$kg m^{-2} s^{-1}$
Void fraction	± 2.5	%
Position of void probes	± 5	µm

3. Results

In this section, measured CHF values and the void fraction at CHF and their parametric trends are presented. Based on the data provided in Table 3, a correlation for the void fraction close to the wall at CHF is then derived. Data was obtained from experiments with mass flux density ranging from G = 500 - 2000 $kg m^{-2} s^{-1}$, which corresponds to superficial liquid flow veloci- ties of 0.3 - 1.2 m s^{-1}. Subcooling nominally ranged from ΔT_{sub} = 4 - 31 K. CHF values for these conditions varied between $\dot{q}$ = 318.0 - 238.6 kW m−2. Void fractions at CHF ranged from 49.7 % to 86.2 %.

Similar to other works in the literature [6, 34], CHF is defined as the maximum heat flux density observed in the experiments. For each thermocouple row the respective CHF value and its time stamp is extracted from the data. Void fraction values at critical heat flux are obtained using the time stamp of CHF for each thermocouple row. Then, the average values for heat flux and void fraction are calculated for all rows. Due to the relatively short length and small width of the heater compared to the channel diameter, there is no significant feedback of the two-phase flow on the boiling process. Additionally, the very high thermal conductivity of copper leads to a nearly isothermal behavior along the direction of flow with almost identical temperature profiles between each thermocouple row. Hence, the averaging of the data over the three measurement positions shown in Fig. 4 was deemed applicable.

3.1. Critical heat flux data

Fig. 5(a) shows the relationship between the measured CHF values and mass flux density for specific values of subcoolings. A linear increase in CHF is observed for higher mass flux density paired with a possible slight increase in slope for higher subcooling. This is in accordance with general parametric trends observed by other authors [35]. Fig. 5(b) shows the parametric trend of CHF for a change in subcooling. For a subcooling of ΔT_{sub} > 9 K, a linear trend in the magnitude of CHF is observed with a slope that increases with higher mass flux density. This parametric trend is similarly found in literature [36, 37]. Extrapolating linear fits to CHF values obtained at

subcoolings ΔT_{sub} > 9 K towards saturation temperature, a common value of $\dot{q} \approx 212$ kW m^{-2} is found. However, measurements close to saturation temperature show a significantly higher value for CHF. The average increase is approximately 12 % compared to values obtained at a subcooling of ΔT_{sub} = 9 K. While some authors have reported a deviation from a linear relationship for small subcooling [38], there is currently no viable explanation for the observed increase in CHF close to saturation conditions.

Table 3**.** Data points used for developing a new correlation for the void fraction at CHF close to the wall.

G kg m^{-2} s^{-1}	ΔT_{sub} K	α_{CHF} –	$\dot{q}$ kWm^{-2}	T_W ^oC
1003.4	30.9	0.556	310.9	82.8
1030.9	30.8	0.505	309.8	83.2
516.8	29.6	0.499	291.6	83.4
1482.1	29.1	0.517	317.5	84.7
1031.1	28.9	0.512	302.4	84.4
2022.9	23.9	0.578	318.0	90.1
468.6	23.9	0.497	274.1	84.5
1486.5	23.7	0.564	298.5	85.7
1017.6	23.6	0.551	285.9	86.1
1484.2	23.5	0.561	296.2	86.2
528.2	23.4	0.515	281.5	84.5
993.1	23.3	0.529	284.7	83.5
2058.5	22.9	0.552	307.6	87.1
500.3	13.8	0.672	256.3	84.5
1985.8	12.5	0.683	269.0	90.0
1014.8	12.2	0.627	246.2	86.9
1436.3	8.9	0.743	245.4	89.0
477.4	8.9	0.743	232.6	89.1
949.3	8.5	0.727	238.6	89.4
953.9	8.2	0.819	244.2	92.7
577.2	4.1	0.862	262.1	99.7
988.6	4.4	0.852	274.8	99.9

3.2. Void fraction data

Fig. 6(a) shows the overview of void fraction experiments with constant subcooling where mass flux density was varied between G = 500 - 2000 kg m−2 s−1. For high subcooling, void fraction increases linearly with increasing mass flux density. This linear influence appears to become less pronounced for subcooling of ΔTsub ≤ 9 K. Fig. 6(b) shows the measured void fraction for different subcoolings for all mass flux densities of this study. It is evident that even in the immediate vicinity of the wall subcooling has a strong effect on void fraction. Compared to mass flux density, subcooling appears to be the prevalent parameter influencing the magnitude of void close to the wall at CHF. In contrast to the weak linear dependency on mass flux density, the void fraction with respect to subcooling can be approximated using an exponential function. In the context of heat transfer phenomena occurring at CHF, the high influence of subcooling suggests that even in the immediate vicinity of the heated surface down to a distance of 100 µm away, there still exists a coupling between bulk flow subcooling and the relevant sublayer at the wall.

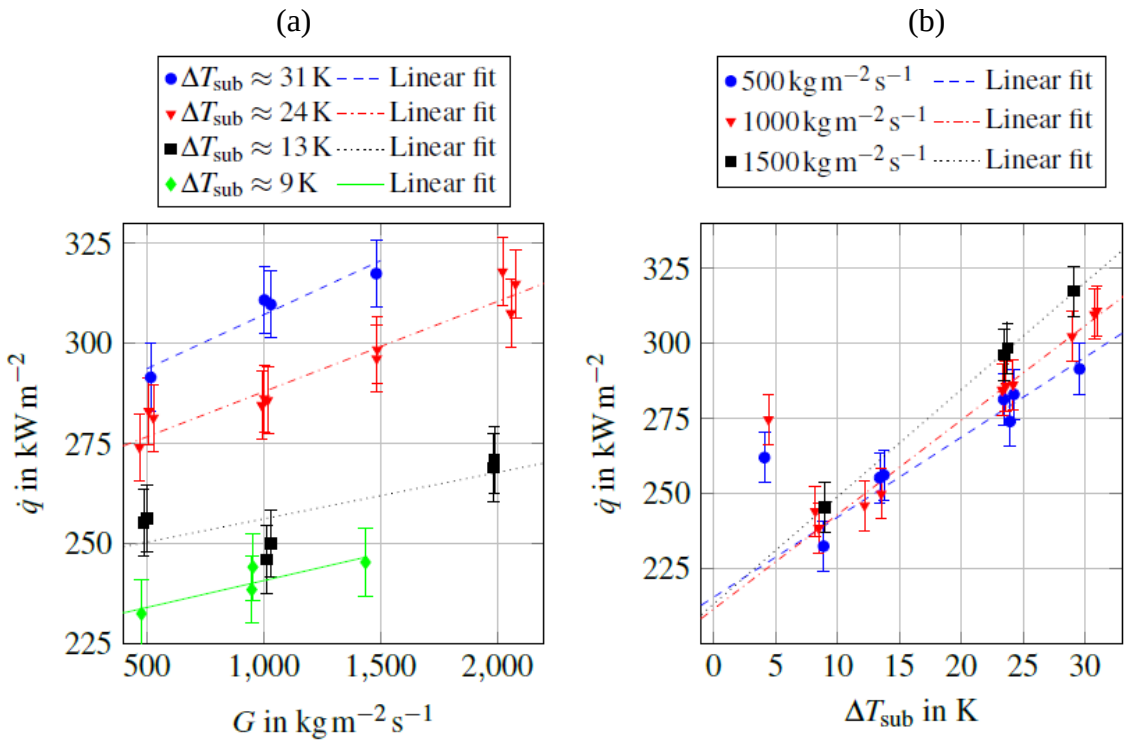

Figure 5. (a) Dependency of CHF on mass flux density for constant subcoolings, (b) Dependency of CHF on subcooling for constant mass flux densities.

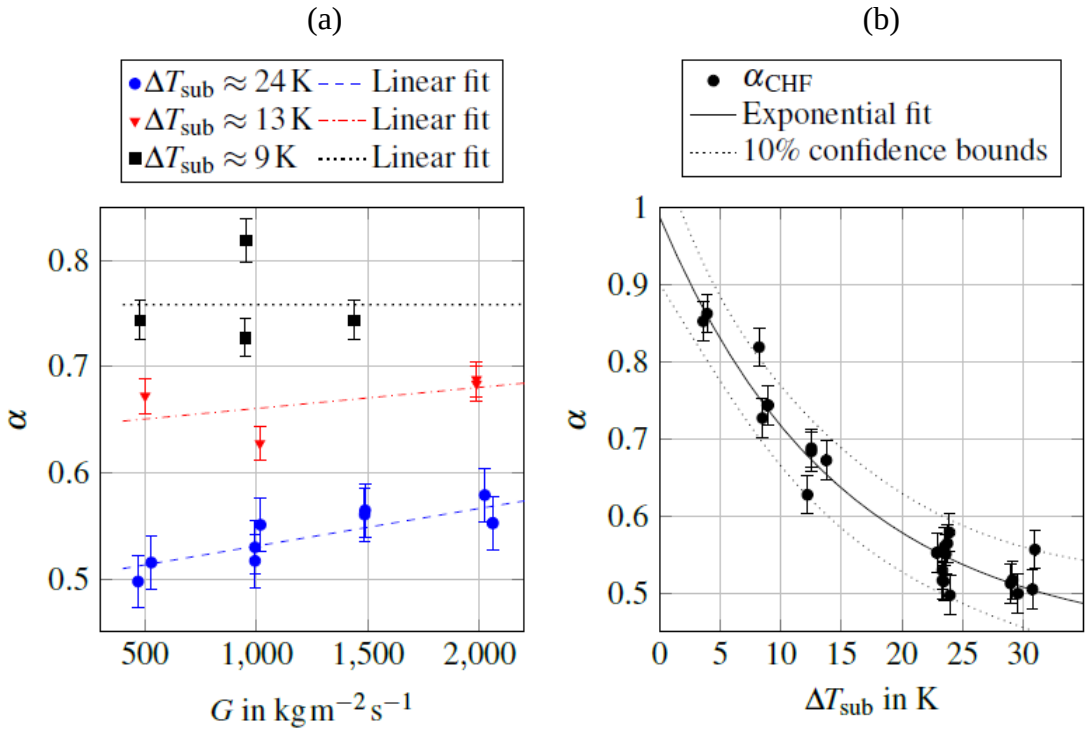

Figure 6. (a) Dependency of CHF on mass flux density for constant subcoolings, (b) Dependency of CHF on subcooling for constant mass flux densities.

4. Proposed correlation

Based on the data presented, a correlation for the void fraction at CHF close to the wall for low boiling refrigerants was developed. The main parametric trends forming the basis for this correlation can be summarized as follows.

1. Void fraction at CHF shows a weak increase for increasing mass flux density.
2. The influence of mass flux density becomes less pronounced for low subcooling.
3. Inlet subcooling has a strong influence on the void fraction at CHF.
4. Void fraction at CHF has an exponential dependency on subcooling.

Drawing on these findings, the functional dependencies were derived to be $\alpha(G,\Delta T_{\mathrm{sub}}) = c_1 + c_2\,\Delta T_{\mathrm{sub}}\,G$ for mass flux density and $\alpha(\Delta T_{\mathrm{sub}}) = c_3 + c_4 \exp(-c_5\,\Delta T_{\mathrm{sub}})$ for subcooling, where $c_{1\text{-}5}$ are arbitrary constant parameters to be determined through a fitting algorithm. As void fraction at CHF is governed by both mass flux density and subcooling, the final correlation will hence be a superposition of these two functional dependencies as shown in Eq. (5).

$$\alpha(G,\Delta T_{sub}) = a + b\,\exp(-c\Delta T_{sub}) + d\Delta T_{sub}G \tag{5}$$

Using a non-linear least squares fitting algorithm from the curve fitting toolbox of MATLAB®, the constant coefficients a, b, c and d in Eq. (5) were determined. As shown in Fig. 7(a), the correlation spans a two-dimensional plane with subcooling and mass flux density as the independent variables. The coefficient of determination - in this case defined as 1 minus the ratio between the sum of the squared residuals and the sum of squared deviations from the mean of the proposed correlation is R^2 = 95.7 %. Within its application limits of 500 kg $m^{-2}s^{-1} \leq G \leq$ 2000 kg $m^{-2}s^{-1}$ and 4 K $\leq \Delta T_{sub} \leq$ 31 K it well reflects the observed behavior of a constant void fraction for saturation conditions and an increasing influence of mass flux density for higher subcooling. A parity plot of the void fractions calculated by Eq. (6) compared to the measured void fractions from the experiment is shown in Fig. 7(b). With the exception of only a few data points, the calculated void fractions at CHF lie well within a 5 % bound. The final correlation was found to be

$$\alpha_{crit}(G,\Delta T_{sub}) = 0.393 + 0.605\,\exp(-0.06782\Delta T_{sub}) + 1.068\times10^{-6}\,\triangle\,T_{sub}G \tag{6}$$

with G in kg m^{-2} s^{-1} and ΔT_{sub} in K. The root-mean-square error of the correlation is *RMSE* = 2.59 %. As no comparable data for the void fraction at CHF at this distance from the wall was found in literature, no further comparison of the correlation's applicability was possible. Therefore, the authors intentionally refrain from presenting the correlation in dimensionless form to avoid indiscriminating usage with other fluids.

5. Conclusions

The eRPI model in combination with CFD is one of the most widely used tools in industry to predict CHF. At the core of the CHF modeling approach lies a switch mechanism based on a constant value of local wall void fraction. In contrast, experiments showed that void fractions close to the wall at CHF are far from constant. Experiments with a wide range of operating parameters were performed to provide void fractions at CHF at distances down to 100 µm from the wall. Using this data, a correlation for the void fraction at the wall at CHF for a low boiling refrigerant was developed. The correlation developed in this study shows good agreement with experimental data and can accurately reproduce the measured void fractions. The addition of a

more precise CHF indicator in current numerical tools has the potential to yield a much better prediction accuracy of CHF until a unifying mechanism is found.

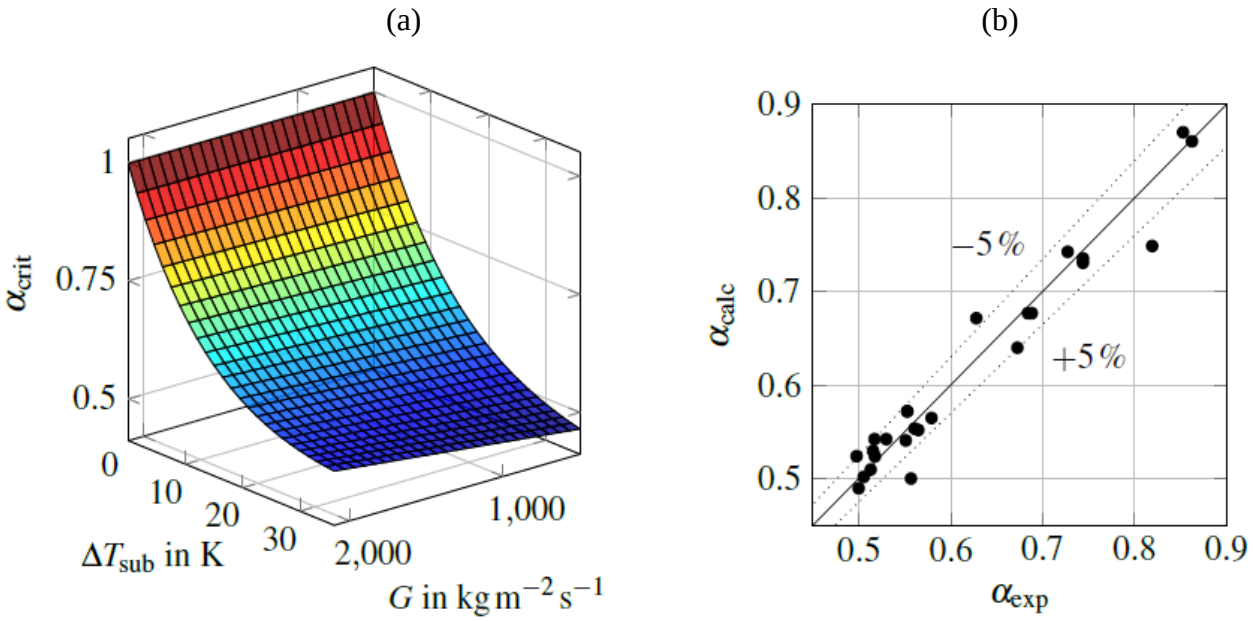

Figure 7. (a) Planar view of the proposed correlation for the void fraction close to the wall at CHF, (b) Parity plot comparing the calculated void fractions at CHF to the measured void fractions.

Acknowledgements

The authors are grateful for the financial support by the Federal Ministry of Economic Affairs and Energy (BMWi) who fund this research under the funding code 1501473A. Responsibility for the content of this report lies with the authors.

References

[1] Y. M. Kwon and S. H. Chang, An Improved Mechanistic Model to Predict Critical Heat Flux in Subcooled and Low Quality Convective Boiling, Journal of the Korean Nuclear Society, vol 31(2), pp. 236 – 255, 1999.

[2] J. Weisman and B. Pei, Prediction of critical heat flux in flow boiling at low qualities, Inter- national Journal of Heat and Mass Transfer, vol 26(10), pp. 1463 – 1477, 1983.

[3] C. H. Lee, I. Mudawar, A Mechanistic Critical Heat Flux Model for Subcooled Flow Boiling Based on Local Bulk Flow Conditions, International Journal of Multiphase Flow, vol 14, pp. 711 – 728, 1988.

[4] G. P. Celata, M. Cumo, A. Mariani, M. Simoncini and G. Zummo, Rationalization of Existing Mechanistic Models for the Prediction of Water Subcooled Flow Boiling Critical Heat Flux, International Journal of Heat Mass Transfer, vol 37, pp. 347 – 360, 1994.

[5] J. Galloway and I. Mudawar, CHF Mechanism in Flow Boiling from a Short Heated Wall - II. Theoretical CHF Model, International Journal of Heat and Mass Transfer, vol 36, pp. 2527 – 2540, 1993.

[6] G. Bloch, M. Bruder and T. Sattelmayer, A study on the mechanisms triggering the departure from nucleate boiling in subcooled vertical flow boiling using a complementary experimental approach, International Journal of Heat and Mass Transfer, vol 92, pp. 403 – 413, 2016.

[7] M. Bruder, G. Bloch and T. Sattelmayer, Critical Heat Flux in Flow Boiling - Review of the Current Understanding and Experimental Approaches, Heat Transfer Engineering, vol 38(3), pp. 347 – 360, 2017.

[8] T. Theofanous, J. Tu, A. Dinh and T. Dinh, The boiling crisis phenomenon: Part I: nucleation and nucleate boiling heat transfer, Experimental Thermal and Fluid Science, vol 26(67), pp. 775 – 792, 2002.

[9] T. Theofanous, T. Dinh, J. Tu and A. Dinh, The boiling crisis phenomenon: Part II: dryout dynamics and burnout, Experimental Thermal and Fluid Science, vol 26(67), pp. 793 – 810, 2002.

[10] S. J. Ha and H. C. No, A dry-spot model of critical heat flux applicable to both pool boiling and subcooled forced convection boiling, International Journal of Heat and Mass Transfer, vol 41(2), pp. 303 – 311, 1998.

[11] S. J. Ha and H. C. No, A dry-spot model of critical heat flux applicable to both pool boiling and subcooled forced convection boiling, International Journal of Heat and Mass Transfer, vol 43(2), pp. 241 – 250, 2000.

[12] S. Gong, W. Ma and H. Gu, An experimental investigation on bubble dynamics and boiling crisis in liquid films, International Journal of Heat and Mass Transfer, vol 79, pp. 694 – 703, 2014.

[13] J. Jung, S. Kim and J. Kim, Observations of the Critical Heat Flux Process During Pool Boiling of FC-72, Journal of Heat Transfer, vol 136(4), pp. 041501 – 041501–12, 2014

[14] D. E. Kim, J. Song and H. Kim, Simultaneous observation of dynamics and thermal evolution of irreversible dry spot at critical heat flux in pool boiling, International Journal of Heat and Mass Transfer, vol 99, pp. 409 – 424, 2016.

[15] S. Mancin, A. Diani and L. Rossetto, Flow boiling heat transfer, dewetting-rewetting, and dryout visualization of hfos in an asymmetrically heated rectangular plain channel, Applied Thermal Engineering, vol 107(Supplement C), pp. 960 – 974, 2016.

[16] J. Weisman, Letter to the editor on ”Evaluation of subcooled critical heat flux correlations for tubes with and without internal twisted tapes” by F. Inasaka and H. Nariai and ”Consideration of CHF margin prediction by subcooled or low quality CHF correlations” by P. Hejzlar and N.E. Todreas, Nuclear Engineering and Design, vol 163(1), pp. 259 – 261, 1996.

[17] E. Krepper and R. Rzehak, CFD for Subcooled Flow Boiling: Simulation of DEBORA Experiments, Nuclear Engineering and Design, vol 241, pp. 3851–3866, 2011.

[18] C. Lifante, T. Frank and A. Burns, Wall Boiling Modelling Extension Towards Critical Heat Flux, in: The 15th International Topical Meeting on Nuclear Reactor Thermalhydraulics, NURETH-15, Pisa, Italy, May 12-15, 2013.

[19] N. Kurul and M. Podowski, Multidimensional effects in forced convection subcooled boiling, in: Proceedings of the 9th International Heat Transfer Conference, Jerusalem, Israel, 1990.

[20] G. Yeoh, S. Vahaji, S. Cheung and J. Tu, Modeling subcooled flow boiling in vertical channels at low pressures part 2: Evaluation of mechanistic approach, International Journal of Heat and Mass Transfer, vol 75(Supplement C), pp. 754 – 768, 2014.

[21] L. Gilman and E. Baglietto, A self-consistent, physics-based boiling heat transfer modeling framework for use in computational fluid dynamics, International Journal of Multiphase Flow, vol 95(Supplement C), pp. 35 – 53, 2017.

[22] M. Buchholz, H. Auracher, T. Luttich and W. Marquardt, A Study of Local Heat Transfer Mechanisms Along the Entire Boiling Curve by Means of Microsensors, International Journal of Thermal Sciences, vol 45, pp. 269 – 283, 2006.

[23] A. Cartellier, Measurement of Gas Phase Characteristics Using new Monofiber Optical Probes and Real-Time Signal Processing, Nuclear Engineering and Design, vol 184, pp. 393– 408, 1998.

[24] A. Cartellier and E. Barrau, Monofiber Optical Probes for Gas Detection and Gas Velocity Measurements: Conical Probes, International Journal of Multiphase Flow, vol 24, pp. 1265 – 1294, 1998.

[25] E. J. Julia, W. K. Harteveld, R. F. Mudde and H. E. Van den Akker, On the Accuracy of the Void Fraction Measurements Using Optical Probes in Bubbly Flows, Review of Scientific Instruments, vol 76, pp. 1 – 13, 2005.

[26] P. C. Mena, F. A. Rocha, J. A. Teixeira, P. Sechet and A. Cartellier, Measurement of Gas Phase Characteristics Using A Monofibre Optical Probe in a Three-Phase Flow, Chemical Engineering Science, vol 63, pp. 4100 – 4115, 2008.

[27] J. Vejrazka, M. Vecer, S. Orvalho, P. Sechet, M. C. Ruzicka and A. Cartellier, Measurement Accuracy of a Mono-Fiber Optical Probe in a Bubbly Flow, International Journal of Multiphase Flow, vol 36, pp. 533 – 548, 2010.

[28] G. Bloch, M. Bruder and T. Sattelmayer, A Critical Review on the Mechanisms Triggering the DNB in Subcooled Flow Boiling Using a Complementary Experimental Approach, in: Proceedings of the 9th International Conference on Boiling and Condensation Heat Transfer, Boulder, Colorado, April 26-30, 2015.

[29] M. Lehner, D. Mewes, U. Dinglreiter and R. Tauscher, Applied Optical Measurements, Springer, Berlin, 1999.

[30] T. Saito, K. Matsuda, Y. Ozawa, S. Oishi and S. Aoshima, Measurement of Tiny Droplets Using a Newly Developed Optcal Fibre Probe Micro- Fabricated by a Femtosecond Pluse Laser, Measurement Science and Technology, vol 20, pp. 1 – 12, 2009.

[31] H. Auracher and M. Buchholz, Experiments on the Fundamental Mechanisms of Boiling Heat Transfer, Journal of the Brazilian Society of Mechanical Science and Engineering, vol 27, pp. 1 – 22, 2005.

[32] G. Bloch, J. Loth, M. Bruder and T. Sattelmayer, Effects of Turbulence and Longitudinal Vortices on Vapor Distribution and Heat Fluxes in Subcooled Flow Boiling, in: Proceedings of ECI 8th Boiling and Condensation, Lausanne, Switzerland, 2012.

[33] H.-J. Lim, K.-A. Chang, C. B. Su and C.-Y. Chen, Bubble Velocity, Diameter, and Void Fraction Measurements in a Multiphase Flow Using Fiber Optic Reflectometer, Review of Scientific Instruments, vol 79, pp. 1 – 11, 2008.

[34] G. Bloch, W. Muselmann, M. Saier and T. Sattelmayer, A Phenomenological Study on Effects Leading to the Departure From Nucleate Boiling in Subcooled Flow Boiling, International Journal of Heat and Mass Transfer, vol 67, pp. 61 – 69, 2013.

[35] S. G. Kandlikar, Critical Heat Flux in Subcooled Flow Boiling - An Assessment of Current Understanding and Future Directions for Research, Multiphase Science and Technology, vol 13, pp. 207 – 232, 2001.

[36] G. Celata, M. Cumo and A. Mariani, Burnout in highly subcooled water flow boiling in small diameter tubes, International Journal of Heat and Mass Transfer, vol 36(5), pp. 1269 – 1285, 1993.

[37] G. Celata and A. Mariani, CHF and Post-CHF (Post-Dryout) Heat Transfer, Chapter 17, Handbook of Phase Change: Boiling and Condensation, edited by S.G. Kandlikar, M. Shoji and V.K. Dhir, pp. 443–493, 1999.

[38] A. E. Bergles, Subcooled Burnout in Tubes of Small Diameter, ASME Paper 63-WA-182.